**Supporting Information**

# Engineered Semiconductor-Dielectric Interfaces in Polymer Ferroelectric Transistors

Arash Ghobadi[1], Thomas B. Kallalos[1], Indeewari M. Karunarathne[1], Dilan M. Gamachchi[1], Andrew C. Meng[1,3], Joseph C. Mathai[2], Shubhra Gangopadhyay[2], and Suchismita Guha[1,3#]

[1]Department of Physics and Astronomy, University of Missouri, Columbia, MO 65211, USA

[2]Department of Electrical Engineering and Computer Science, University of Missouri, Columbia, MO 65211, USA

[3]MU Materials Science and Engineering Institute, University of Missouri, Columbia, MO 65211, USA

[#]Corresponding author E-mail: guhas@missouri.edu

## Contents

## 1. Output characteristics (PVDF-TrFE and PVDF- HFP)

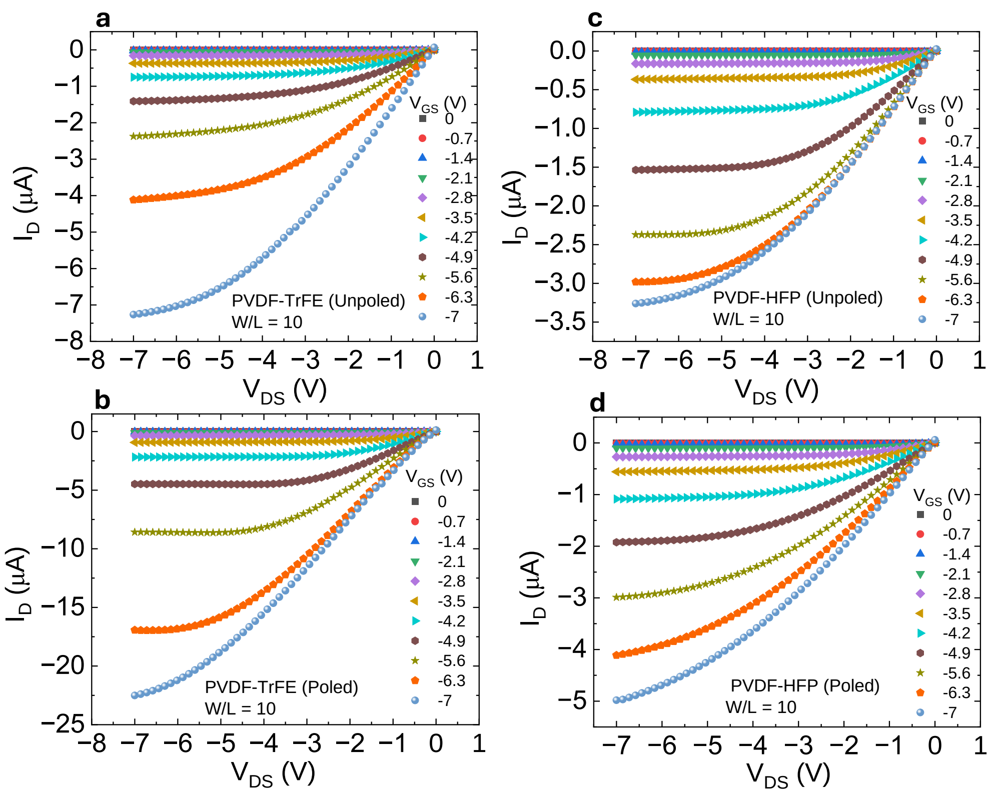


**Fig. S1** Output characteristics of DPP-DTT FETs with (a) unpoled PVDF-TrFE, (b) poled PVDF-TrFE, (c) unpoled PVDF-HFP, and (d) poled PVDF-HFP. The thickness of the dielectric layer is ~ 45 nm.

## 2. Carrier mobilities - poled PVDF-TrFE

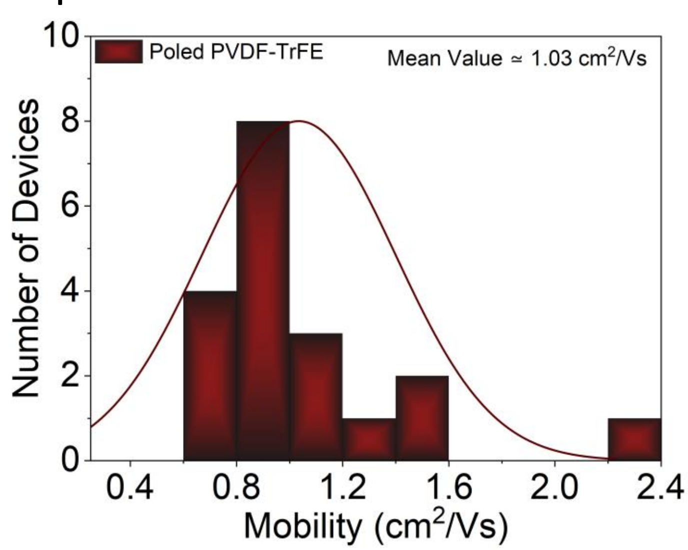


**Fig. S2** Histogram of carrier mobility from vertically poled PVDF-TrFE/DPP-DTT FETs.

## 3. PVDF-TrFE with $Al_2O_3$: current-voltage characteristics

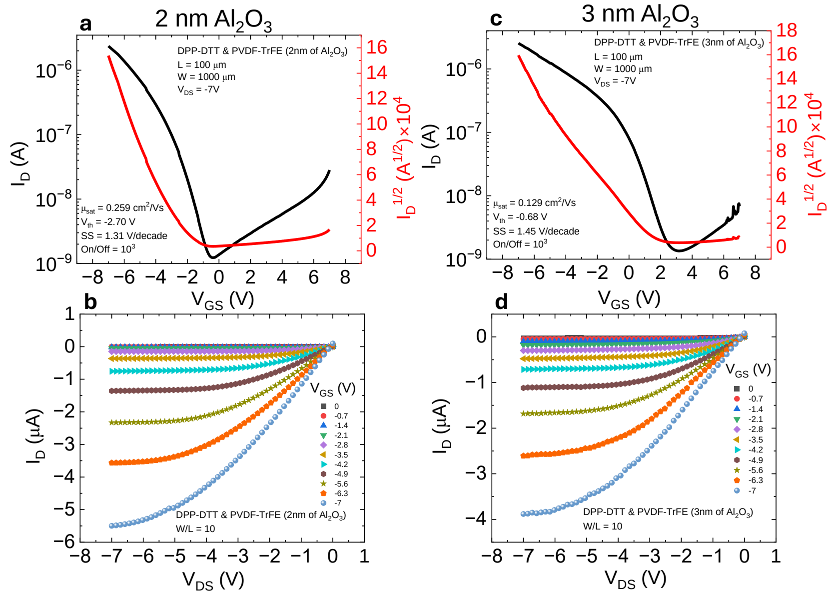

**Fig. S3** Transfer and output characteristics of DPP-DTT/PVDF-TrFE FETs. (a), (b) 2 nm of $Al_2O_3$ on PVDF-TrFE. (c), (d) 3 nm of $Al_2O_3$ on PVDF-TrFE.

## 4. PVDF-HFP with $Al_2O_3$: current-voltage characteristics

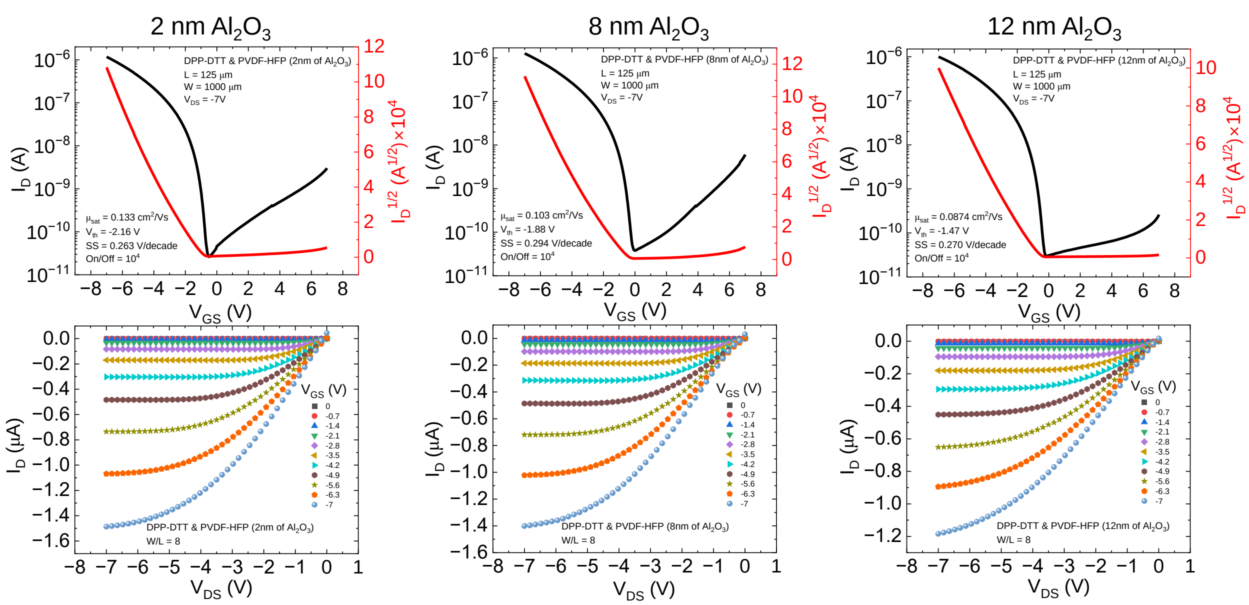

**Fig. S4** Transfer and output characteristics of DPP-DTT/PVDF-HFP FETs. (a), (b) 2 nm of $Al_2O_3$ on PVDF-HFP. (c), (d) 8 nm of $Al_2O_3$ on PVDF-HFP. (c), (d) 8 nm of $Al_2O_3$ on PVD-HFP.

## 5. Device characteristics of PVDF-HFP FETs without $Al_2O_3$

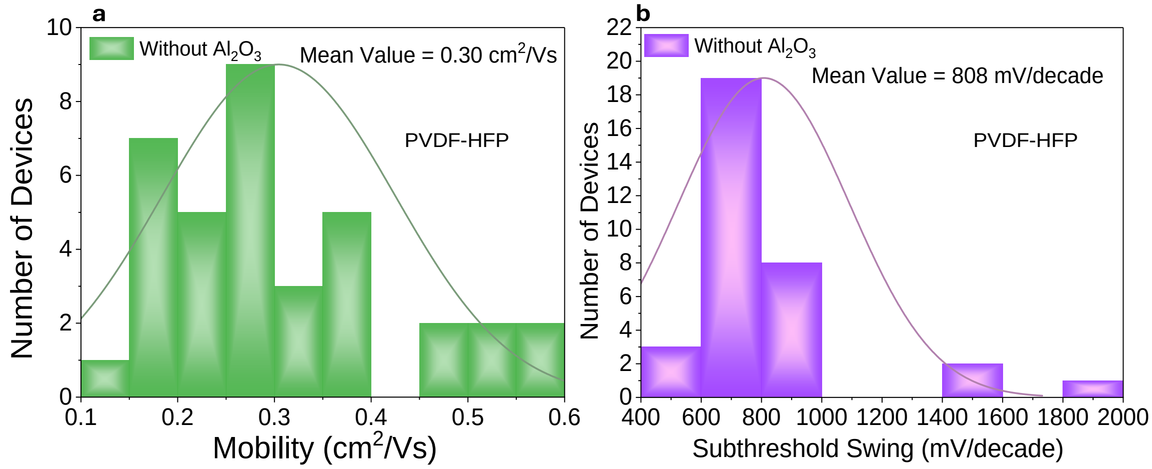


**Fig. S5** (a) Histogram of the $\mu_{sat}$ for PVDF-HFP FETs without $Al_2O_3$. (c) Histogram of SS for PVDF-HFP FETs without $Al_2O_3$.

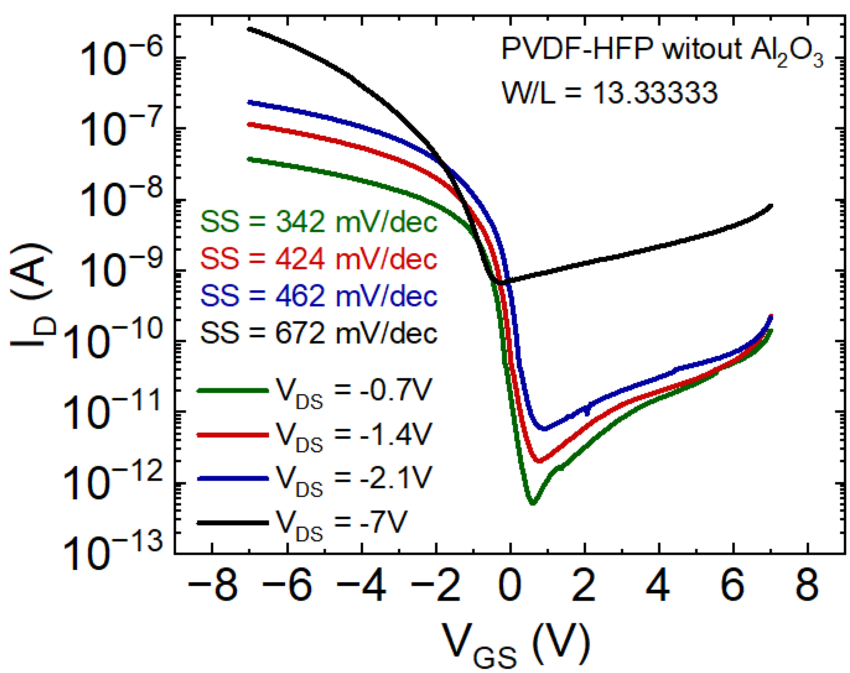


**Fig. S6** Transfer current-voltage characteristics for varying values of $V_{DS}$ for a PVDF-HFP FET without $Al_2O_3$.

## 6. Subthreshold region – transfer characteristics of 2 nm $Al_2O_3$ with PVDF-HFP

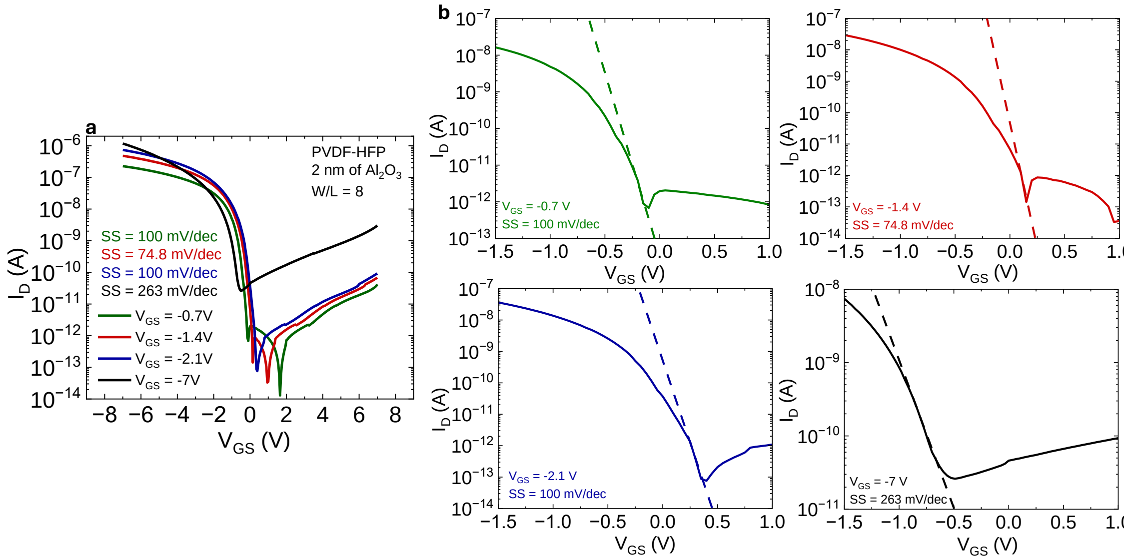


**Fig. S7**. (a) Transfer current-voltage characteristics for varying values of $V_{DS}$ for the PVDF-HFP FET with 2 nm of $Al_2O_3$. (e) Linear fits for obtaining SS for the transfer characteristics shown in (a).

## 7. Interface trap density ($D_{it}$) from capacitance and conductance measurements

The capacitance versus voltage (C-V) and conductance versus voltage (G-V) measurements were carried out from MIS diodes (metal – PVDF-TrFE-DPP-DTT) to compare the interface trap density ($D_{it}$) of the unpoled PVDF-TrFE and the poled PVDF-TrFE. The poling was performed in a similar fashion to the FETs. All measurements were carried out till 10 KHz. The capacitance and conductance values were corrected for the series resistance as outlined in Refs. [1, 2]. **Fig. S8** shows the C-V and G-V curves for the vertically poled PVDF-TrFE and the unpoled PVDF-TrFE MIS diodes. Most organic semiconductors are appropriately modeled by the continuum of states model, where the interface traps are assumed to have energy levels that are so closely spaced across the band gap and as such, could be treated as a continuum of states. The equivalent parallel conductance ($G_P$) using the continuum of states model extracted at different biases from the measured capacitance and conductance is given by:

$$\frac{G_p}{\omega} = \frac{qD_{it}\ln(1+\omega^2\tau^2)}{2\omega\tau}, \qquad (1)$$

where $\tau$ is the interface time constant and $G_p/\omega$ has a maximum at $\omega\tau$=1.98.

Using a negative to positive sweep, the flat-band (FB) voltage of both MIS diodes ~ 0.75 V. A clear loss peak is absent in either of the devices, suggesting that it is mainly dominated by capture and emission of carriers by the gate bias independent of bulk traps with a slight contribution from interface states. The $D_{it}$ values were obtained by using Eq. (1) and plotted in **Fig. S9** for both poled and unpoled PVDF-TrFE based MIS.

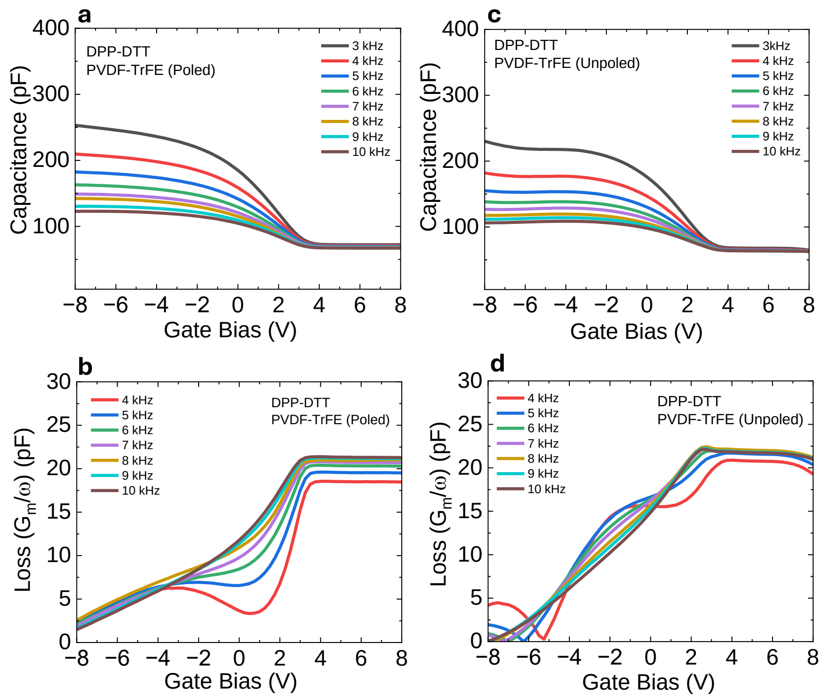


**Fig. S8**. C-V and G-V curves for poled PVDF-TrFE/DPP-DTT MIS (a, b) and for unpoled PVDF-TrFE/DPP-DTT MIS (c, d).

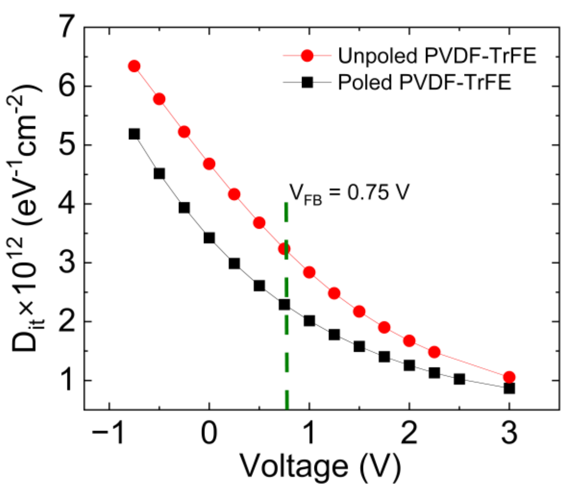


**Fig. S9**. Interface trap density ($D_{it}$) estimated from the depletion region in DPP-DTT MIS diodes with poled and unpoled PVDF-TrFE.

## 8. Atomic layer deposition of $Al_2O_3$ on PVDF-HFP and PVDF-TrFE

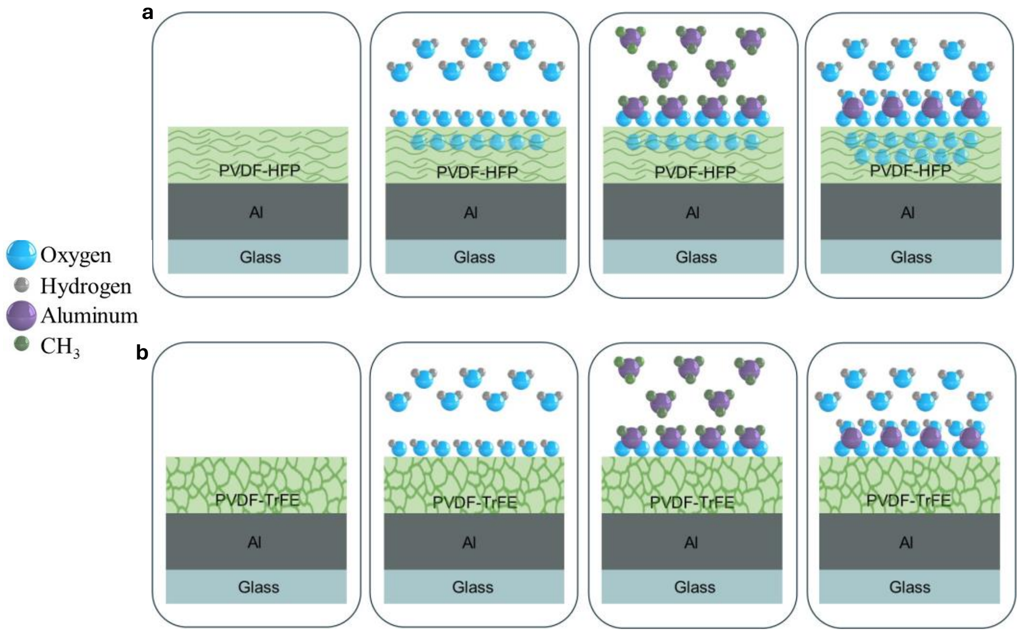


**Fig. S10** ALD process for the growth of $Al_2O_3$ on (a) PVDF-HFP and (b) PVDF-TrFE.

## 9. Subthreshold swing and other FET parameters from literature

Table S1: FET architectures and properties using different semiconductors and dielectrics.

| Structure | Semiconductor | Dielectric (Thickness) | Carrier Mobility ($cm^2$/Vs) | *SS* (V/dec) | Ref |
|---|---|---|---|---|---|
| BGTC | Pentacene | cross-linked CR-V (120 nm) | 0.62 | 0.185 | [3] |
| BGBC | PDPPTT | BST-P(VDF-HFP) | 0.14 | 0.221 | [4] |
| BGBC | TIPS-Pentacene/PαMS | BST-P(VDF-HFP) | 0.06 | 0.169 | [4] |
| BGBC | TIPS-Pentacene/PαMS | BZ-P(VDF-HFP) | 0.08 | 0.153 | [4] |
| BGTC | Pentacene | CEP-PMMF (251 nm) | 1.07 | 0.066 | [5] |
| BCTG | pBTTT-C16 | P(VDF-TrFE-CFE) (160 nm) | 0.4 | 0.097 | [6] |
| BGBC | TIPS-Pentacene | PVP (3 layers) (400 nm) | 0.95 | 0.300 | [7] |
| BGBC | TIPS-Pentacene | PVCN (130 nm) /P(VDF-TrFE-CFE) (290 nm) | | 0.080 | [8] |
| BGTC | Pentacene | TiO2 | 0.15 | 0.170 | [9] |
| BGBC | DPh-BTBT | Ti/$TiO_X$/SAM | 1.8 | 0.059 | [10] |
| BGBC | DPh-DNTT | Ti/$TiO_X$/SAM | 3.0 | 0.063 | [10] |
| BGBC | DPh-DNTT | Al/$AlO_X$/SAM | 4.6 | 0.071 | [10] |

BGTC: bottom gate top contact; BGBC: bottom gate bottom contact; BCTG: bottom contact top gate; BGBC: bottom gate bottom contact

## 10. STEM images and EDS maps

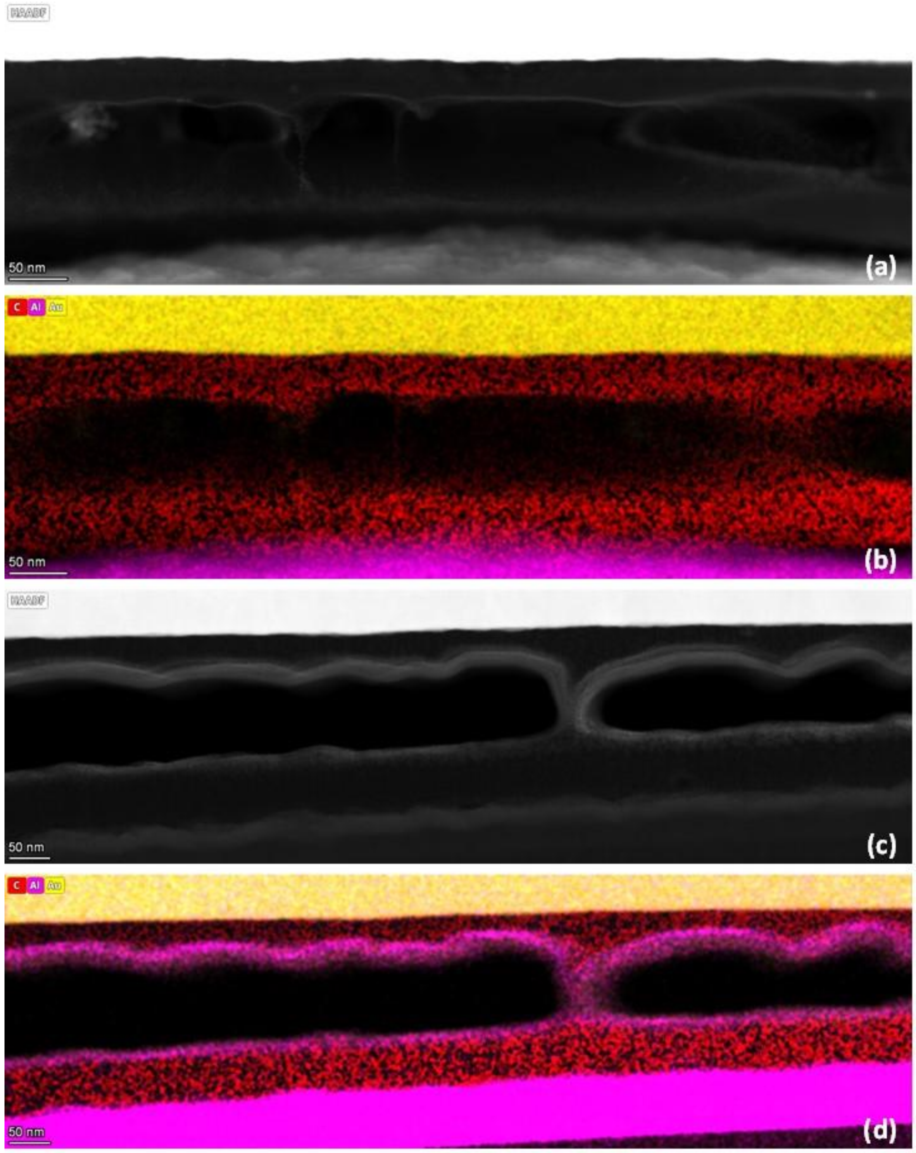


**Fig. S11** PVDF-HFP without $Al_2O_3$ a) HAADF-STEM image and b) STEM-EDS map; PVDF-HFP with $Al_2O_3$ c) HAADF-STEM image and d) STEM-EDS map. There are some holes in these samples due to ion beam induced damage during the lamella thinning process.

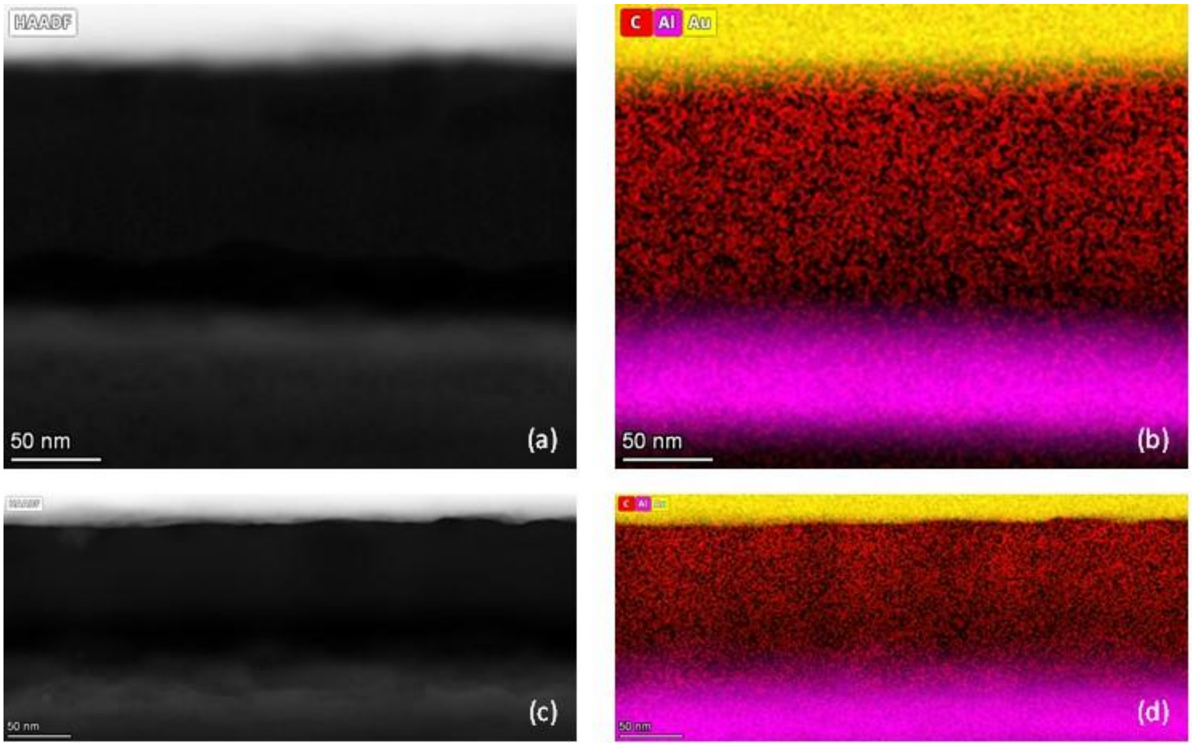


**Fig. S12** PVDF-HFP without $Al_2O_3$ a) HAADF-STEM image and b) STEM-EDS map; PVDF-HFP with $Al_2O_3$ c) HAADF-STEM image and d) STEM-EDS map; these samples are significantly thicker than those in Fig. S11, and the $Al_2O_3$ is not visible.

Likely, the $Al_2O_3$ layer is not visible due to warping in the sample due to delamination at the Al/PVDF-HFP interface as confirmed by weaker C signal in the EDS map.

## 11. AFM Images

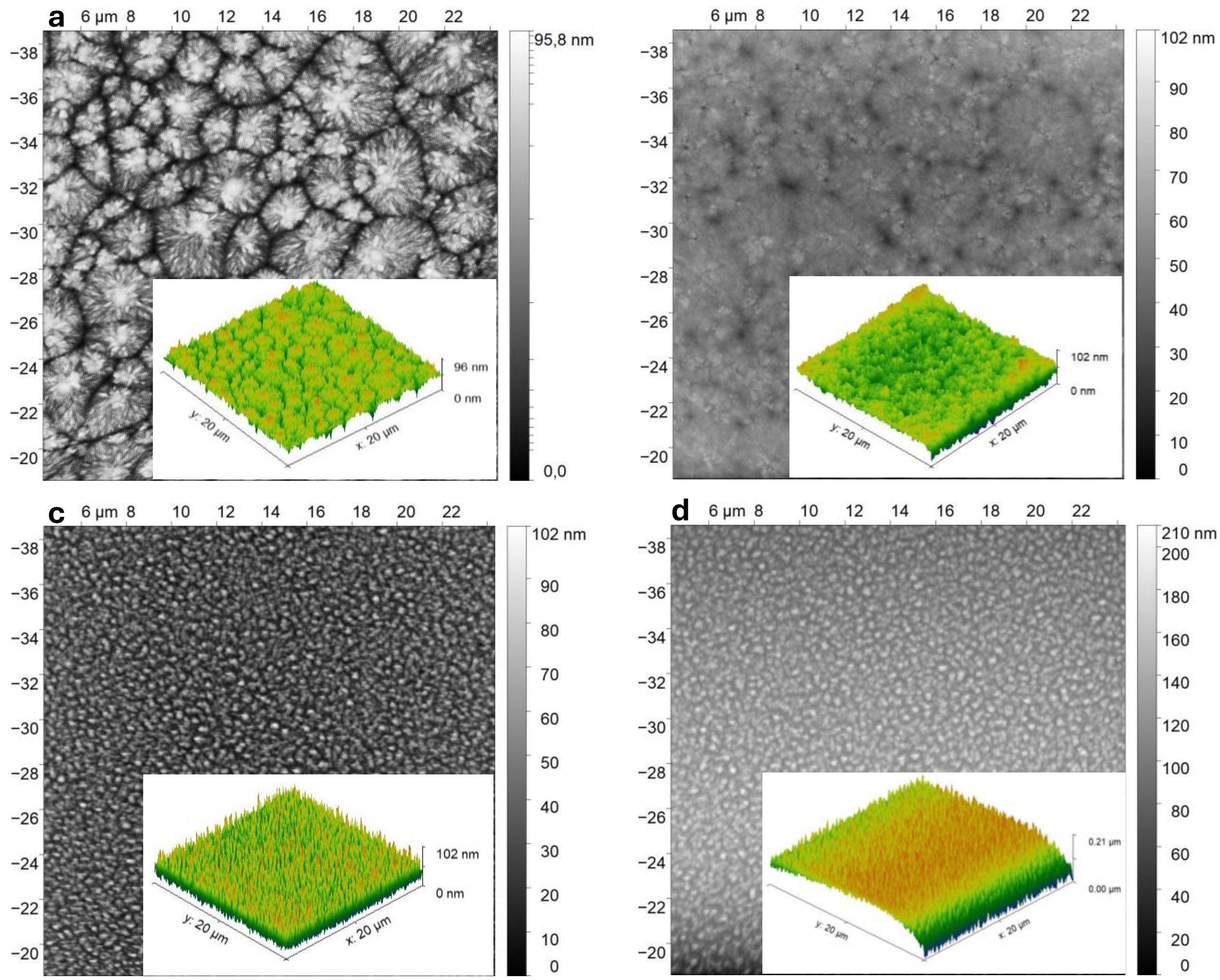


**Fig. S13** AFM images from (a) PVDF-TrFE film with no $Al_2O_3$, (b) PVDF-TrFE film with 12 nm of $Al_2O_3$, (c) PVDF-HFP film with no $Al_2O_3$, and (d) PVDF-HFP film with 12 nm $Al_2O_3$. The insets show 3D AFM images.

## 12. Ferroelectric properties of PVDF-based copolymers

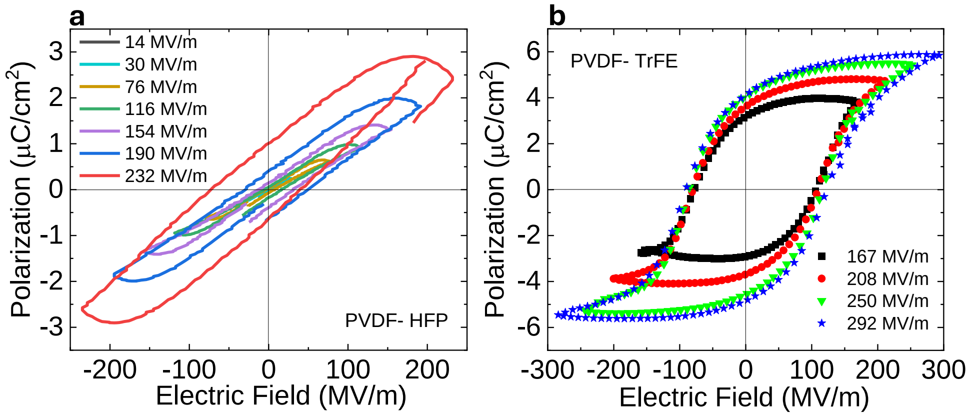


**Fig. S14** (a) Polarization versus electric field for a PVDF-HFP capacitor. (b) Polarization versus electric field for a PVDF-TrFE capacitor. Reproduced with permission from Ref. [11]. Copyright 2025, John Wiley and Sons.

References:


1. M. Yun, S. Gangopadhyay, M. Bai, H. Taub, M. Arif and S. Guha, *Org. Electron.*, 2007, **8**, 591-600.
2. E. H. Nicollian and J. R. Brews, *MOS (Metal Oxide Semiconductor) Physics and Technology*, Wiley: New York, 2003.
3. S. H. Kim, S. Y. Yang, K. Shin, H. Jeon, J. W. Lee, K. P. Hong and C. E. Park, *Appl. Phys. Lett.*, 2006, **89**.
4. S. Faraji, T. Hashimoto, M. L. Turner and L. A. Majewski, *Org. Electron.*, 2015, **17**, 178-183.
5. W. Xu and S.-W. Rhee, *Org. Electron.*, 2010, **11**, 996-1004.
6. J. Li, Z. Sun and F. Yan, *Adv. Mater.*, 2012, **24**, 88-93.
7. S. Conti, S. Lai, P. Cosseddu and A. Bonfiglio, *Adv. Mater. Technol.*, 2017, **2**, 1600212.
8. W. Tang, Y. Fu, Y. Huang, Y. Li, Y. Song, X. Xi, Y. Yu, Y. Su, F. Yan and X. Guo, *npj Flex Electron*, 2022, **6**, 18.
9. L. A. Majewski, R. Schroeder and M. Grell, *Adv. Funct. Mater.*, 2005, **15**, 1017-1022.
10. M. Geiger, R. Lingstädt, T. Wollandt, J. Deuschle, U. Zschieschang, F. Letzkus, J. N. Burghartz, P. A. van Aken, R. T. Weitz and H. Klauk, *Adv. Electron. Mater.*, 2022, **8**, 2101215.
11. E. Restuccia, A. Ghobadi and S. Guha, *Adv. Mater. Interf.*, 2025, **n/a**, 2401035.